

The Role of the Schwinger Effect in Superradiant Axion Lasers

Bradley Shapiro*

Department of Physics and Astronomy, Dartmouth College, Hanover, NH 03755

(Dated: March 4, 2025)

Superradiance can cause the axion cloud around a rotating black hole to reach extremely high densities, and the decay of these axions can produce a powerful laser. The electric field of these lasers is strong enough that the Schwinger effect may become significant, resulting in the production of an electron-positron plasma. We explore the dynamics between axion lasers and this electron-positron plasma. While there are several mechanisms by which the inclusion of a plasma can impact the laser's behavior, the most significant of these mechanisms is that the electron-positron plasma imparts an effective mass on the photon. As the plasma frequency increases, axion decay becomes energetically unfavorable, up to the point where the axion no longer decays into photons, shutting off the laser. We find that the impact of the electron-positron plasma on the dynamics of the system depend heavily on the parameters, specifically the axion mass m_ϕ and the superradiant coupling α , and that we may divide parameter space into three regimes: the unenhanced, enhanced, and unstable regimes. In the unenhanced and enhanced regime, the system will eventually settle into an equilibrium state, emitting a laser of constant luminosity while the number of axions remains constant. In the unenhanced regime, this equilibrium state can be calculated while neglecting the effects of Schwinger production; in the enhanced regime, the equilibrium luminosity is slightly larger than what it would be without Schwinger production. In the unstable regime, the electron-positron plasma suppresses axion decay to the point where the system is never able to reach equilibrium; instead, the axions continue to grow superradiantly. In all three cases, the production of superradiant axions will eventually cause the black hole to spin down to the point where superradiance ceases.

I. INTRODUCTION

The axion has emerged as a leading candidate for dark matter [1–4]. A topic of significant research interest is the idea that axions might be detected around rotating black holes [5–9], via superradiance, which allows for the extraction of energy and angular momentum from a rotating black hole [10–12]. Superradiance is often understood through the concept of a gravitational atom [13, 14], as, in Kerr spacetime, the Klein-Gordon equation permits quasi-bound state solutions, characterized by integer quantum numbers (n, ℓ, m) , much like those around a hydrogen atom. For a massive scalar field, these quasi-bound states have energy [12]

$$E_n = \text{Re}(\omega_n) = m_\phi \left(1 - \frac{\alpha^2}{2(n + \ell + 1)^2} \right), \quad (1)$$

where m_ϕ is the scalar mass and the coupling parameter is

$$\alpha = \frac{Gm_\phi M_{BH}}{\hbar c} = .037 \left(\frac{m_\phi}{10^{-5} \text{ eV}} \right) \left(\frac{M_{BH}}{10^{24} \text{ kg}} \right). \quad (2)$$

Importantly, unlike in hydrogen atoms, where the frequency is entirely real, the quasi-bound states around rotating black holes may have a complex frequency, $\text{Im}(\omega_n) \neq 0$. Depending on the sign of this imaginary frequency, the state will experience either exponential growth or exponential decay proportional to $e^{\text{Im}(\omega_n)t}$. States with exponential growth are referred to as superradiant.

Conceptually, there are a number of ways to understand superradiance. [15] showed that, when a wave is incident on a rotating body, the second law of thermodynamics requires, under certain conditions, that the wave be reflected back with greater energy and angular momentum than it initially had. From a particle perspective, superradiance may be understood as a consequence of the Penrose process, whereby an object passing through the ergosphere of a rotating black hole may extract energy and angular momentum from the black hole. In either picture, this energy extraction can only occur through the creation of new particles, because the quasi-bound nature of the aforementioned states means that individual particles cannot become more energetic. Consequently, superradiance increases the population of particles around the black hole. The aforementioned descriptions are classical in nature, i.e. the scalar field is not

* bradley.e.shapiro.gr@dartmouth.edu

quantized, which is how superradiance is usually treated. However, there do exist some treatments of superradiance as a quantum phenomenon [16, 17]. These offer some additional insight into the exact mechanism in which superradiant particles are created around a black hole.

In models that include an axion, rotating black holes are therefore expected to produce a dense axion cloud via superradiance. In [18], the authors propose that, in certain regions of parameter space, these axions can undergo stimulated decay into photons, creating a powerful laser, which they refer to as a BLAST (*Black hole Lasers powered by Axion Superradiant instabilities*). These BLASTs are powerful enough that the Schwinger effect becomes significant.

The Schwinger effect refers to a quantum mechanical, non-perturbative process whereby a strong electromagnetic field produces electron-positron pairs. In the case of BLASTs, [18] speculated that the Schwinger effect would create an electron-positron plasma, which would eventually make axion decay energetically impossible, thereby shutting off the laser. They speculated that this would result in the axion laser shutting off and then restarting in a periodic fashion, but they did not explore the underlying dynamics in detail. These dynamics are quite important, as they determine whether BLASTs will be intermittent or continuous, or indeed whether they will occur at all.

This paper is structured as follows. In section 2, we review how BLASTs behave in the absence of the Schwinger effect. In section 3, we explore how an electron-positron plasma evolves in the superradiant axion cloud around a rotating black hole, and how that plasma affects the behavior of the photons and axions in that cloud. In section 4, we analyze the resulting Boltzmann equations. Section 5 is the conclusion.

II. BLASTS WITHOUT SCHWINGER PRODUCTION

We begin by briefly summarizing the work of [18]. Note that some numerical values differ from those given in [18], because we parameterize quantities in terms of $\frac{\alpha}{.037}$, whereas [18] parameterizes quantities in terms of $\frac{\alpha}{.03}$.

For scalar fields, the fastest-growing state is the $2p$ -state ($n = 2, \ell = m = 1$). The $2p$ -state is approximately toroidal in shape, with the following dimensions:

$$\text{Major radius:} \quad \langle r \rangle = \frac{5\hbar}{cm_\phi\alpha} = 2.6 \left(\frac{\alpha}{0.037} \right)^{-1} \left(\frac{m_\phi}{10^{-5} \text{ eV}} \right)^{-1} \text{ m} \quad (3)$$

$$\text{Minor radius:} \quad \Delta r = \frac{\sqrt{5}\hbar}{cm_\phi\alpha} = 1.2 \left(\frac{\alpha}{0.037} \right)^{-1} \left(\frac{m_\phi}{10^{-5} \text{ eV}} \right)^{-1} \text{ m} \quad (4)$$

$$\text{Volume:} \quad V = 2\pi^2 \langle r \rangle \Delta r^2 = 71 \left(\frac{\alpha}{0.037} \right)^{-3} \left(\frac{m_\phi}{10^{-5} \text{ eV}} \right)^{-3} \text{ m}^3 \quad (5)$$

$$\text{Surface area:} \quad A = 4\pi^2 \langle r \rangle \Delta r = 120 \left(\frac{\alpha}{0.037} \right)^{-2} \left(\frac{m_\phi}{10^{-5} \text{ eV}} \right)^{-2} \text{ m}^2. \quad (6)$$

In the $2p$ -state, axions grow superradiantly at a rate

$$\Gamma_s = \frac{c^2 \tilde{a} \alpha^8 m_\phi}{24\hbar} = 2.2 * 10^{-3} \tilde{a} \left(\frac{\alpha}{0.037} \right)^8 \left(\frac{m_\phi}{10^{-5} \text{ eV}} \right) \text{ s}^{-1}, \quad (7)$$

where \tilde{a} is the black hole's spin parameter. At the same time, axions decay into photons at a rate

$$\Gamma_\phi = 1.1 * 10^{-49} K^2 \left(\frac{m_\phi}{10^{-5} \text{ eV}} \right)^5 \text{ s}^{-1}, \quad (8)$$

where $K \sim \mathcal{O}(1)$ is a model-dependent factor. Due to the quasi-bound nature of the $2p$ -state, axions will not leave the $2p$ -cloud except when disturbed by outside forces. However, a photon produced inside the $2p$ -cloud will naturally exit the $2p$ -cloud at the speed of light, producing an escape rate of

$$\Gamma_\gamma = \frac{c}{\Delta r} = 2.5 * 10^8 \left(\frac{\alpha}{0.037} \right) \left(\frac{m_\phi}{10^{-5} \text{ eV}} \right) \text{ s}^{-1}. \quad (9)$$

[18] found that the Boltzmann equations for the total number of photons and axions in the $2p$ -cloud to be

$$\frac{dN_\phi}{dt} = \Gamma_s N_\phi - \Gamma_\phi (N_\phi(1 + C_1 N_\gamma) - C_2 N_\gamma^2) \quad (10)$$

$$\frac{dN_\gamma}{dt} = -\Gamma_\gamma N_\gamma + 2\Gamma_\phi (N_\phi(1 + C_1 N_\gamma) - C_3 N_\gamma^2), \quad (11)$$

where

$$C_1 = \frac{8\alpha^2}{25} \quad C_2 = \frac{2\alpha^4}{75} \quad C_3 = C_2 + \alpha C_1. \quad (12)$$

$\Gamma_\gamma \gg \Gamma_s \gg \Gamma_\phi$, and so for low values of N_γ and N_ϕ photon production is negligible. In this regime, N_ϕ grows exponentially, $N_\phi \sim e^{\Gamma_s t}$, while $N_\gamma \sim \frac{2\Gamma_\phi}{\Gamma_\gamma} N_\phi$. However, when $N_\gamma \gtrsim \frac{1}{C_1}$, the $C_1 N_\gamma$ terms become significant, which increases the rate at which axions decay into photons; this marks the beginning of lasing. In this regime, N_γ increases rapidly, while N_ϕ 's growth slows, until both reach their equilibrium values:

$$N_\gamma^{\text{eq}} = \frac{\Gamma_s}{C_1 \Gamma_\phi} = 4.8 * 10^{49} \tilde{a} K^{-2} \left(\frac{\alpha}{0.037} \right)^6 \left(\frac{m_\phi}{10^{-5} \text{ eV}} \right)^{-4} \quad (13)$$

$$N_\phi^{\text{eq}} = \frac{\Gamma_\gamma}{2C_1 \Gamma_\phi} = 2.7 * 10^{60} K^{-2} \left(\frac{\alpha}{0.037} \right)^{-1} \left(\frac{m_\phi}{10^{-5} \text{ eV}} \right)^{-4}. \quad (14)$$

In the process of reaching these equilibrium values, the photon number reaches a maximum value of

$$N_\gamma^{\text{max}} \approx \frac{\Gamma_s}{C_1 \Gamma_\phi} \ln \frac{\Gamma_s}{\Gamma_\phi} = 5.1 * 10^{51} \tilde{a} K^{-2} \left(\frac{\alpha}{0.037} \right)^6 \left(\frac{m_\phi}{10^{-5} \text{ eV}} \right)^{-4} \left(\frac{\xi}{106} \right), \quad (15)$$

where

$$\xi = \ln \frac{\Gamma_s}{\Gamma_\phi} = 107 - 4 \ln \left(\frac{m_\phi}{10^{-5} \text{ eV}} \right) + 8 \ln \left(\frac{\alpha}{0.037} \right) + \ln \left(\frac{\tilde{a}}{K^2} \right). \quad (16)$$

This corresponds to a peak luminosity of

$$L^{\text{max}} = \frac{m_\phi}{2} N_\gamma^{\text{max}} \Gamma_\gamma = 1.0 * 10^{43} \tilde{a} K^{-2} \left(\frac{\alpha}{0.037} \right)^7 \left(\frac{m_\phi}{10^{-5} \text{ eV}} \right)^{-2} \left(\frac{\xi}{106} \right) \text{ erg/s}. \quad (17)$$

This luminosity is comparable to that of the entire Milky Way galaxy. These BLASTs, if they exist, are therefore of great experimental interest, as they should be observable and could provide insight into both primordial black holes and scalar dark matter.

III. ELECTRON-POSITRON PLASMAS IN BLASTS

[18] showed that the number of photons generated by a BLAST is so great that the electric field inside the $2p$ -cloud will approach the critical Schwinger field. It is expected that, in this limit, the production of electron-positron pairs via the Schwinger effect will be significant. In the resulting electron-positron plasma, the photon has an effective mass equal to the plasma frequency. For a sufficient density of electrons and positrons, this will result in axions being energetically incapable of decaying into photons. At the same time, the dynamics of the plasma are nontrivial. In this section, we explore the behavior of this plasma, and the effect it has on axion decay. From this point onward, we will work in natural units where $c = \hbar = \epsilon_0 = 1$.

A. Rate of Schwinger production

The Schwinger effect [19, 20] is a nonperturbative effect caused by vacuum decay in the presence of an electromagnetic field. The Schwinger effect can only occur if $E^2 - B^2$ and $\vec{E} \cdot \vec{B}$ are nonzero; consequently, a single beam of light cannot induce the Schwinger effect. However, when multiple beams of light intersect, the interference of the two electromagnetic fields may satisfy the requirements for Schwinger production [21, 22]; this is an area of significant research interest, as it is hoped that the Schwinger effect may be observable at the focus of two lasers (for a review, see [23]). In the same way, Schwinger production may occur inside the $2p$ -cloud, where a large number of photons are traveling in different directions.

For simplicity, we make two approximations. The first is that we ignore the magnetic field in calculating the rate of Schwinger production. This is common for research on the Schwinger effect at the intersection of laser beams, e.g. [21–25], for the reason that the Schwinger effect cannot occur in a pure magnetic field (i.e., zero electric field), whereas it can occur in a pure electric field (i.e., zero magnetic field). However, it should be noted that the contribution of the

magnetic field can be significant in situations like the one we are modeling, and it tends to reduce the rate of Schwinger production by 1-2 orders of magnitude [26]. The second approximation we make is that we neglect the effect of axions on the Schwinger effect; it has been shown that the presence of axions can enhance the Schwinger effect by several orders of magnitude [27]. Thus, our two approximations have opposite effects (increasing and decreasing the rate of Schwinger production), so that, while it is unclear whether our calculated pair production rate is an overestimate or an underestimate, it is likely accurate to the true value to within 1-2 orders of magnitude. The following should therefore only be understood as a rough order-of-magnitude estimate, which may be refined in future research.

In the case of a constant, uniform electric field, electron-positron pairs are created at a rate per unit volume of

$$\frac{dn_{e^+e^-}}{dt} = \frac{e^2 E^2}{4\pi^3} \sum_{n=1}^{\infty} \frac{1}{n^2} e^{-\pi \frac{E_c}{E} n}, \quad (18)$$

where $E_c = 1.3 * 10^{18}$ V/m is the critical Schwinger field. In general, the Schwinger effect is highly dependent on the space- and time-dependence of the electric field, i.e. a nonconstant and/or nonuniform field will produce electrons and positrons at a very different rate than the figure given above. However, the effects of nonconstancy and nonuniformity are most pronounced when the electric field varies on length- and time-scales less than the Compton wavelength, λ_C [28].

In our case, the random decay of axions into photons results in a superposition of an enormous number of electric fields, so that the total electric field within the $2p$ -cloud will be highly inhomogeneous and impossible to predict. However, the length- and time-scales of these inhomogeneities will be the wavelength of the light, which is $\frac{2}{m_\phi}$. For all axion masses that are of interest as a dark matter candidate, this is far greater than the Compton wavelength. Therefore we may divide the $2p$ -cloud into a number of patches, each with volume equal to the Compton volume λ_C^3 , and in each patch we may treat the electric field as uniform and constant. (It should be noted that most research on the Schwinger effect at the intersection of laser beams is done under the assumption of high-frequency light, typically X-rays, and in such cases this approximation does not hold. We are taking advantage of the fact that the light in a BLAST is at a much lower frequency than what would be practical in an earth-based experiment.) Therefore, the total rate of Schwinger pair production throughout the $2p$ -cloud is

$$\frac{dN_{e^+e^-}}{dt} = \sum_{\text{patches}} \lambda_C^3 \frac{e^2 E^2}{4\pi^3} \sum_{n=1}^{\infty} \frac{1}{n^2} e^{-\pi \frac{E_c}{E} n}. \quad (19)$$

If one wished, one could now find the average value of the electric field in the $2p$ -cloud, and substitute this value into the above equation. However, this approach would not produce an accurate estimate of the rate of Schwinger production. This is because of the Schwinger effect's highly nonlinear nature, meaning that even slight increases to the electric field may result in a dramatic increase to the rate of pair production. This is significant in our case, because we have an electric field that is, effectively, randomly varying, and as such there will be some patches where the electric field strength is greater or less than the $2p$ -cloud's average field strength. These "hotspots" and "coldspots" contribute more than average and less than average, respectively, to pair production. If the Schwinger effect were linear, the hotspots and coldspots would cancel out when averaging over the patches, and therefore they could be ignored. However, the Schwinger effect's nonlinear nature means that the surplus of pair production in the hotspots will be far greater than the deficit in pair production in the coldspots. Consequently, if we were to use the average value of E , we would significantly underestimate the rate of pair production. What we do instead is find the probability distribution of the electric field throughout the $2p$ -cloud, $f(E)$. Our total rate of pair production will then be

$$\frac{dN_{e^+e^-}}{dt} = V \int_0^{\infty} dE f(E) \frac{e^2 E^2}{4\pi^3} \sum_{n=1}^{\infty} \frac{1}{n^2} e^{-\pi \frac{E_c}{E} n}. \quad (20)$$

To find $f(E)$, we assume that the electric field components are normally distributed uncorrelated random variables with equal standard deviation, σ_{EM} . The electric field magnitude $E = \sqrt{E_x^2 + E_y^2 + E_z^2}$ then follows a chi distribution, with probability density

$$f(E) = \frac{\sqrt{2}}{\sqrt{\pi} \sigma_{EM}^3} E^2 e^{-\frac{E^2}{2\sigma_{EM}^2}}. \quad (21)$$

σ_{EM} may be found from the energy density, which in terms of the electromagnetic field components is

$$u = \frac{1}{2} (E_x^2 + E_y^2 + E_z^2 + B_x^2 + B_y^2 + B_z^2), \quad (22)$$

and therefore

$$\langle u \rangle = 3\sigma_{\text{EM}}^2 = \frac{m_\phi N_\gamma}{2V}. \quad (23)$$

Thus the rate of pair production is

$$\frac{dN_{e^+e^-}}{dt} = \frac{3\sqrt{3}\pi e^2 E_c^5 V^{\frac{5}{2}}}{64\sqrt{m_\phi^3 N_\gamma^3}} \sum_{n=1}^{\infty} n^3 G_{03}^{30} \left(\frac{3\pi^2 E_c^2 V}{4m_\phi N_\gamma} n^2 \middle|_{-\frac{5}{2}, -2, 0} \right) \equiv \Gamma_{\text{Schw}}, \quad (24)$$

where G is the Meijer G-function. For every electron-positron pair produced, the electromagnetic field loses energy $2m_e$, resulting in the loss of photons at a rate of $\frac{4m_e}{m_\phi} \Gamma_{\text{Schw}}$.

We can see that Schwinger production is parameterized by $\frac{N_\gamma}{N_\gamma^{\text{Schw}}}$, where

$$N_\gamma^{\text{Schw}} = \frac{3\pi^2 E_c^2 V}{4m_\phi} = 4.9 * 10^{51} \left(\frac{\alpha}{0.037} \right)^{-3} \left(\frac{m_\phi}{10^{-5} \text{ eV}} \right)^{-4}. \quad (25)$$

For $N_\gamma \lesssim N_\gamma^{\text{Schw}}$, Γ_{Schw} is well approximated by

$$\Gamma_{\text{Schw}} \approx \frac{e^2 E_c^2 V}{4\sqrt{3}\pi} \sum_{n=1}^{\infty} e^{-3 \left(\frac{N_\gamma}{n^2 N_\gamma^{\text{Schw}}} \right)^{\frac{-1}{3}}} \left(\frac{N_\gamma}{n^2 N_\gamma^{\text{Schw}}} \right)^{\frac{1}{3}}. \quad (26)$$

We will find that, for our purposes, N_γ is always less than N_γ^{Schw} , and therefore we may freely use this approximation.

B. Positron/Electron Escape Rate

Just as photons will exit the $2p$ -cloud at a rate Γ_γ , we also must calculate the rate at which electrons and positrons will exit the $2p$ -cloud. Schwinger pairs are created with some initial momentum, but we assume that this is negligible compared to the momentum imparted by radiation pressure. This radiation pressure is driven by an energy flux, which we assume to be constant throughout the $2p$ -cloud and which is given by $F = \frac{L}{A} = \frac{3m_\phi}{4V} N_\gamma$. Let ρ be a coordinate defined as the distance from the ring running through the center of the $2p$ -torus; we expect that radiation pressure will cause electrons and positrons to move predominantly in the $\hat{\rho}$ direction. Therefore each electron and positron gains energy at a rate

$$\frac{3\sigma_T m_\phi N_\gamma}{4V} = \frac{d}{dt} \frac{m_e}{\sqrt{1 - \left(\frac{d\rho}{dt} \right)^2}}. \quad (27)$$

We assume that the timescale on which an individual electron or positron accelerates is much shorter than the timescale over which N_γ changes, and therefore we may treat N_γ as constant. From this we find that the time T_{e^\pm} that it takes for the electron or positron to leave the $2p$ -cloud is given by

$$\Delta r - \rho_0 = T_{e^\pm} \sqrt{1 - \frac{16m_e^2 V^2}{9\sigma_T^2 m_\phi^2 N_\gamma^2 T_{e^\pm}^2}} - \frac{4m_e V}{3\sigma_T m_\phi N_\gamma} \tan^{-1} \left(\sqrt{\frac{9\sigma_T^2 m_\phi^2 N_\gamma^2 T_{e^\pm}^2}{16m_e^2 V^2} - 1} \right) \quad (28)$$

where ρ_0 is the value of ρ where the electron or positron was created. While it is not possible to get an exact analytical expression for T_{e^\pm} in terms of ρ_0 , the above equation can be numerically inverted, so that in principal we may calculate the escape rate as

$$\Gamma_{e^\pm} = \frac{1}{\langle T_{e^\pm} \rangle} = \frac{\Delta r^2}{2 \int_0^{\Delta r} T_{e^\pm} \rho_0 d\rho_0}. \quad (29)$$

Notably, in the limit $\frac{3\sigma_T m_\phi}{4V m_e} \Delta r N_\gamma \rightarrow \infty$, $\Gamma_{e^\pm} \rightarrow \Gamma_\gamma$; this represents the limit where the radiation pressure is so great that it immediately accelerates electrons and positrons to relativistic velocities. We may therefore use

$$\chi \equiv \frac{3\sigma_T m_\phi}{4V m_e} \Delta r N_\gamma = \frac{N_\gamma}{6.2 * 10^{40}} \left(\frac{\alpha}{0.037} \right)^2 \left(\frac{m_\phi}{10^{-5} \text{ eV}} \right)^3 \quad (30)$$

as a dimensionless parameter for the behavior of Γ_{e^\pm} . Γ_{e^\pm} increases monotonically as χ increases, asymptotically approaching Γ_γ . This behavior is analyzed in greater detail in the appendix, and it is plotted in Fig. 1a.

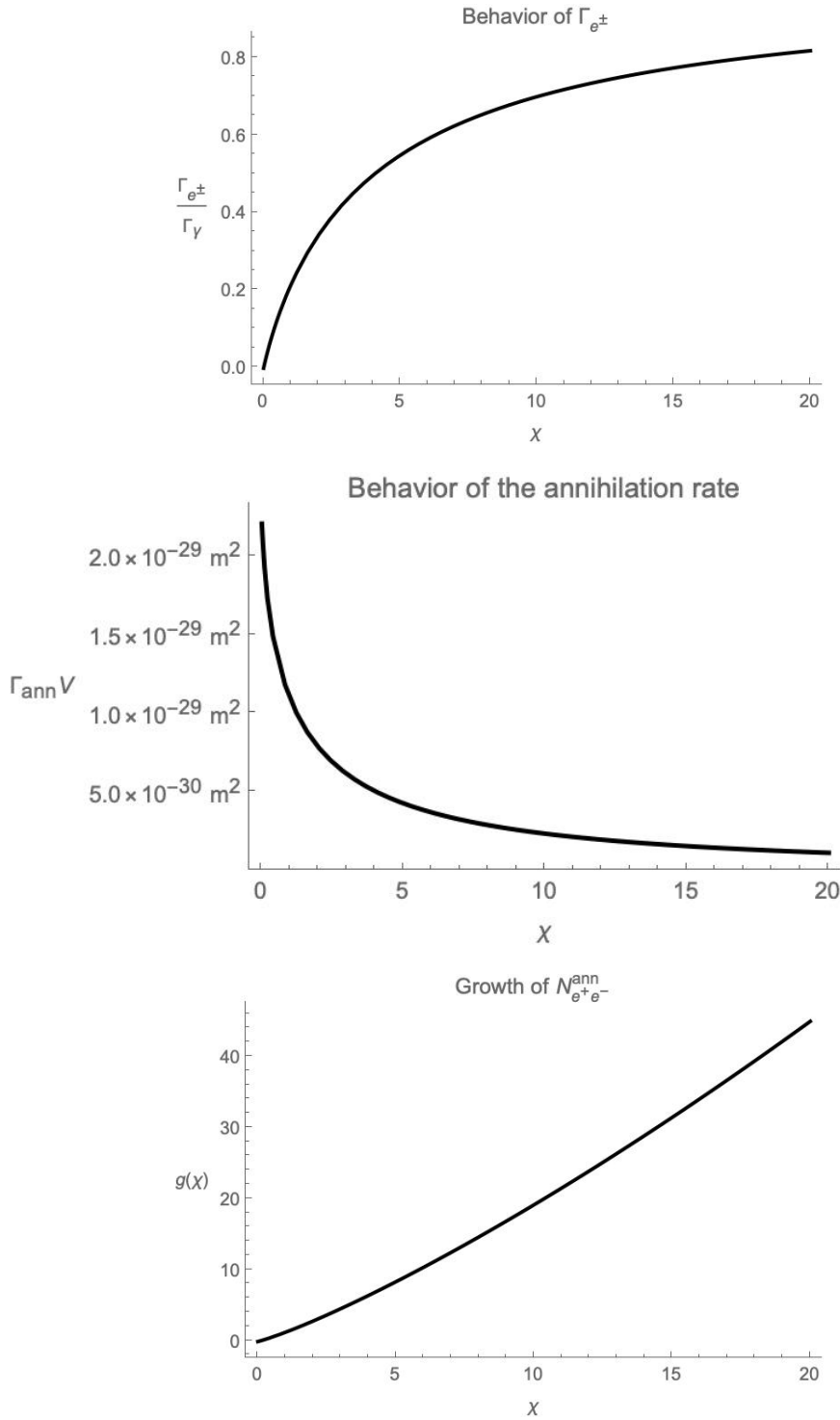


FIG. 1. Plot of functions of χ , which parameterizes how relativistic the electrons and positrons become as a result of radiation pressure. (a) demonstrates the behavior of Γ_{e^\pm} . At low χ , there is negligible radiation pressure driving electrons and positrons to exit the $2p$ -cloud, and so $\Gamma_{e^\pm} \rightarrow 0$. For large χ the electrons and positrons are quickly accelerated to very close to the speed of light, causing them to exit the $2p$ -cloud at roughly the same rate as the photons, and as a result $\Gamma_{e^\pm} \rightarrow \Gamma_\gamma$. (b) demonstrates the behavior of Γ_{ann} . Slower particles present a larger cross-section, and therefore pair annihilation occurs frequently for small χ but vanishes as $\chi \rightarrow \infty$. Note that Γ_{ann} is the rate of annihilation per number of pairs squared, not the total rate; in practice, large χ will correlate with large $N_{e^+e^-}$, so the total rate of annihilation will increase with χ . (c) demonstrates the behavior of $g(\chi)$, which scales the number of electron-positron pairs at which annihilation becomes relevant. We show in the appendix that, for large χ , $g(\chi)$ grows as $\frac{\chi^2}{(\ln \chi)^2}$.

C. Pair Annihilation

Within the electron-positron plasma, some number of electrons and positrons will annihilate and produce two photons. The cross-section of this annihilation is given by [29, 30]

$$\sigma(v_{\text{com}}) = \frac{3\sigma_T(1-v_{\text{com}})^2}{32v_{\text{com}}} \left(\frac{3-v_{\text{com}}^4}{v_{\text{com}}} \ln \frac{1+v_{\text{com}}}{1-v_{\text{com}}} - 2(2-v_{\text{com}}^2) \right), \quad (31)$$

where v_{com} is the velocity of the electron and positron in the center-of-mass frame. Due to the effects of radiation pressure, described in the previous section, we expect the electrons and positrons are primarily moving in the $\hat{\rho}$ direction; we may therefore treat the electron-positron plasma as a series of beams, each pointed in the $\hat{\rho}$ direction. For a pure beam of positrons and a pure beam of electrons with velocities v_{e^+} and v_{e^-} , respectively, each of which is pointed in the same direction, the rate of annihilation is

$$\frac{dn_{e^\pm}}{dt} = -n_{e^+}n_{e^-}|v_{e^+} - v_{e^-}|\sigma(v_{\text{com}}), \quad (32)$$

The center-of-mass velocity is related to the electron's and positron's velocities by

$$v_{\text{com}} = \sqrt{\frac{\gamma_{e^+}\gamma_{e^-}(1-v_{e^+}v_{e^-})-1}{\gamma_{e^+}\gamma_{e^-}(1-v_{e^+}v_{e^-})+1}}, \quad (33)$$

where γ_{e^\pm} are the Lorentz factors corresponding to v_{e^\pm} .

In our case, the electrons and positrons have a distribution of velocities, $f(v)$, and therefore the total rate of annihilation is

$$\frac{dn_{e^\pm}}{dt} = -n_{e^+}n_{e^-} \int dv_{e^+}dv_{e^-} f(v_{e^+})f(v_{e^-})|v_{e^+} - v_{e^-}|\sigma(v_{\text{com}}). \quad (34)$$

Using the same approach as in the previous section, the velocity of an electron or positron is directly related to the length of time it has existed, t :

$$t = \frac{1}{\sqrt{1-v^2}} \frac{4m_e V}{3\sigma_T m_\phi N_\gamma} = \frac{\Delta r}{\chi\sqrt{1-v^2}}, \quad (35)$$

and therefore we may relate the velocity of the electron or positron to the distance it has traveled since it was created, which we call $\Delta\rho$:

$$\Delta\rho = \frac{\Delta r}{\chi} \left(\frac{v}{\sqrt{1-v^2}} - \tan^{-1} \frac{v}{\sqrt{1-v^2}} \right). \quad (36)$$

As in the previous section, we cannot write an analytic expression for v in terms of $\Delta\rho$, but it is still possible in principle to express the former as a function of the latter, $v(\Delta\rho)$. We may therefore replace our integral over the velocities of the electron and positron with an integral over the locations at which the two particles are created and at which the annihilation occurs. Assuming that electrons and positrons are created uniformly throughout the $2p$ -torus, and that annihilation occurs uniformly throughout the $2p$ -torus, we get that the rate of annihilation is

$$\frac{dn_{e^\pm}}{dt} = -n_{e^+}n_{e^-} \int_0^{\Delta r} d\rho \frac{2\rho}{\Delta r^2} \int_0^\rho d\rho_{0e^+} \frac{2\rho_{0e^+}}{\rho^2} \int_0^\rho d\rho_{0e^-} \frac{2\rho_{0e^-}}{\rho^2} |v_{e^+} - v_{e^-}|\sigma(v_{\text{com}}), \quad (37)$$

where v_{e^\pm} is a function of $\rho - \rho_{0e^\pm}$. In this integral, ρ represents the coordinate at which annihilation occurs, and ρ_{0e^\pm} represents the coordinate at which the electron or positron was created. The factors of $\frac{2\rho}{\Delta r^2}$ and $\frac{2\rho_{0e^\pm}}{\rho^2}$ are the probability distributions for ρ and ρ_{0e^\pm} . Since the number of electrons and positrons is assumed to be equal, we may write this as

$$\frac{dN_{e^+e^-}}{dt} = -\frac{8N_{e^+e^-}^2}{V\Delta r^2} \int_0^{\Delta r} d\rho \int_0^\rho \int_0^\rho d\rho_{0e^+}d\rho_{0e^-} \frac{\rho_{0e^+}\rho_{0e^-}}{\rho^3} |v_{e^+} - v_{e^-}|\sigma(v_{\text{com}}) \equiv -\Gamma_{\text{ann}}N_{e^+e^-}^2. \quad (38)$$

We show in the appendix that $\Gamma_{\text{ann}}V$ is a function only of χ , which is displayed in Fig. 1b. As χ increases, the electrons and positrons become more relativistic, and so both the cross section and the rate of annihilation decrease.

Each pair annihilation creates two photons, and therefore there ought to be a $\Gamma_{\text{ann}}N_{e^+e^-}^2$ term in the photon Boltzmann equation. However, these photons will have energy of at least m_e , whereas the photons created by axion decay have energy $\frac{m_\phi}{2} \ll m_e$. A rigorous analysis will therefore require us to keep track of two separate photon populations, low-energy photons produced by axion decay and high-energy photons produced by pair annihilation; the $\Gamma_{\text{ann}}N_{e^+e^-}^2$ term would appear in the Boltzmann equation of the latter, but not the former. However, as we will show later, pair annihilation does not occur at a significant rate, and therefore we may ignore these high-energy photons.

D. Suppression of Axion Decay

Lastly, we must account for the effects of the electron-positron plasma on axion decay. The plasma frequency is given by

$$\omega_p = \sqrt{\frac{2e^2N_{e^+e^-}}{m_eV}}, \quad (39)$$

and this serves as the effective mass of photons in the $2p$ -cloud. It is a straightforward exercise of QED to show that this scales the rate of axion decay by

$$\Gamma_\phi \rightarrow \Gamma_\phi \text{Re} \sqrt{1 - \frac{8e^2}{m_em_\phi^2V}N_{e^+e^-}} \equiv \Gamma'_\phi. \quad (40)$$

Note that this has the effect of shutting down axion decay entirely when

$$N_{e^+e^-} \geq \frac{m_em_\phi^2V}{8e^2} = 6.5 * 10^{17} \left(\frac{\alpha}{0.037}\right)^{-3} \left(\frac{m_\phi}{10^{-5} \text{ eV}}\right)^{-1} \equiv N_{e^+e^-}^{\text{shutoff}}. \quad (41)$$

IV. BOLTZMANN EQUATIONS AND PARAMETER SPACE

We may now write the Boltzmann equations for the axion number, photon number, and Schwinger pair number:

$$\frac{dN_\phi}{dt} = \Gamma_s N_\phi - \Gamma'_\phi (N_\phi(1 + C_1 N_\gamma) - C_2 N_\gamma^2) \quad (42)$$

$$\frac{dN_\gamma}{dt} = -\Gamma_\gamma N_\gamma + 2\Gamma'_\phi (N_\phi(1 + C_1 N_\gamma) - C_3 N_\gamma^2) - \frac{4m_e}{m_\phi} \Gamma_{\text{Schw}} \quad (43)$$

$$\frac{dN_{e^+e^-}}{dt} = \Gamma_{\text{Schw}} - \Gamma_{e^\pm} N_{e^+e^-} - \Gamma_{\text{ann}} N_{e^+e^-}^2. \quad (44)$$

Initially, the rate of pair production is vanishingly small, so N_ϕ and N_γ behave identically to the description given in [18]. When N_γ gets within a few orders of magnitude of N_γ^{Schw} (roughly $10^{-4}N_\gamma^{\text{Schw}}$), electron-positron pairs begin to be produced, and these electron-positron pairs impact the axion decay rate. Thus we need only consider the case when N_γ is approaching N_γ^{Schw} .

Let us first consider the behavior of $N_{e^+e^-}$. When $N_{e^+e^-}$ is small, the annihilation term is negligible, and so the number of electron-positron pairs is controlled only by the rate of production and the rate of escape. For all $N_\gamma < N_\gamma^{\text{Schw}}$, $\Gamma_{e^\pm} \gg \frac{\Gamma_{\text{Schw}}}{N_\gamma}$, and therefore we may approximate $N_{e^+e^-} \approx \frac{\Gamma_{\text{Schw}}}{\Gamma_{e^\pm}}$. This approximation holds until either annihilation becomes significant, or until N_γ exceeds N_γ^{Schw} . We will show that, in what appears to be a remarkable coincidence, both of these conditions are met at roughly the same time. Examining first the matter of N_γ exceeding N_γ^{Schw} , we note that, when $N_\gamma = N_\gamma^{\text{Schw}}$, χ is given by

$$\chi^{\text{Schw}} = 7.8 * 10^{10} \left(\frac{\alpha}{0.037}\right)^{-1} \left(\frac{m_\phi}{10^{-5} \text{ eV}}\right)^{-1}, \quad (45)$$

and the number of electron-positron pairs is, provided the aforementioned approximation still holds at this point,

$$N_{e^+e^-}^{\text{Schw}} = 8.8 * 10^{48} \left(\frac{\alpha}{0.037}\right)^{-4} \left(\frac{m_\phi}{10^{-5} \text{ eV}}\right)^{-4}. \quad (46)$$

As for pair annihilation, that becomes significant when $N_{e^+e^-} \sim \frac{\Gamma_{e^\pm}}{\Gamma_{\text{ann}}} \equiv N_{e^+e^-}^{\text{ann}}$, which may be written as

$$N_{e^+e^-}^{\text{ann}} = \frac{\Gamma_\gamma V}{\sigma_T} g(\chi) = 2.7 * 10^{30} \left(\frac{\alpha}{0.037} \right)^{-2} \left(\frac{m_\phi}{10^{-5} \text{ eV}} \right)^{-2} g(\chi), \quad (47)$$

where

$$g(\chi) = \frac{\chi^5}{48 \left(\int_0^\chi \hat{T}_{e^\pm} \hat{\rho}_0 d\hat{\rho}_0 \right) \left(\int_0^\chi d\hat{\rho} \int_0^{\hat{\rho}} d\hat{\rho}_{0e^+} \int_0^{\hat{\rho}} d\hat{\rho}_{0e^-} \frac{\hat{\rho}_{0e^+} \hat{\rho}_{0e^-}}{\hat{\rho}^3} |v_{e^+} - v_{e^-}| \frac{\sigma(v_{\text{com}})}{\sigma_T} \right)}, \quad (48)$$

which uses the hat notation defined in the appendix. $g(\chi)$ is plotted in Fig. 1c, and we show in the appendix that its asymptotic form is

$$g(\chi) \xrightarrow{\chi \rightarrow \infty} \frac{2\chi^2}{3(\ln \chi)^2}. \quad (49)$$

This means that, at $\chi = \chi^{\text{Schw}}$, $N_{e^+e^-}^{\text{ann}} \sim N_{e^+e^-}^{\text{Schw}}$. In other words, pair annihilation only becomes relevant right as N_γ reaches N_γ^{Schw} . Thus, in the $N_\gamma < N_\gamma^{\text{Schw}}$ regime, we may ignore annihilation, and the approximation $N_{e^+e^-} \approx \frac{\Gamma_{\text{Schw}}}{\Gamma_{e^\pm}}$ holds.

We now turn to the effects of $N_{e^+e^-}$ on N_ϕ and N_γ . There are two conditions under which the electron-positron plasma may become significant to the dynamics of the photon number and the axion number. The first way is that, as $N_{e^+e^-}$ approaches $N_{e^+e^-}^{\text{shutoff}}$, the rate of axion decay Γ'_ϕ vanishes. This happens when $\frac{\Gamma_{\text{Schw}}}{\Gamma_{e^\pm} N_{e^+e^-}^{\text{shutoff}}} \sim 1$. The second way is that, for sufficiently large N_γ , the rate of photon loss from the Schwinger effect will become significant. This happens when $\frac{4m_e \Gamma_{\text{Schw}}}{m_\phi \Gamma_\gamma N_\gamma} \sim 1$. For all values of N_γ , $\frac{\Gamma_{\text{Schw}}}{\Gamma_{e^\pm} N_{e^+e^-}^{\text{shutoff}}} \gg \frac{4m_e \Gamma_{\text{Schw}}}{m_\phi \Gamma_\gamma N_\gamma}$, and therefore the former condition will be met before the latter. Once the number of electron-positron pairs reaches $N_{e^+e^-}^{\text{shutoff}}$, N_γ ceases to increase, and consequently it will never become large enough for the second condition to be fulfilled. We may therefore neglect the $\frac{4m_e}{m_\phi} \Gamma_{\text{Schw}}$ term in the N_γ Boltzmann equation.

The buildup of Schwinger pairs suppresses the decay of axions into photons, resulting in a lower equilibrium value for the photon number. The equilibrium value may be found by taking the expression from [18] and substituting $\Gamma_\phi \rightarrow \Gamma'_\phi$, which yields the expression

$$N_\gamma^{\text{eq}2} \left(1 - \frac{8e^2 \Gamma_{\text{Schw}}^{\text{eq}}}{m_e m_\phi^2 V \Gamma_{e^\pm}^{\text{eq}}} \right) = N_\gamma^{\text{eq,w/o}2}, \quad (50)$$

where $\Gamma_{\text{Schw}}^{\text{eq}}$ and $\Gamma_{e^\pm}^{\text{eq}}$ represent Γ_{Schw} and Γ_{e^\pm} evaluated at N_γ^{eq} , and $N_\gamma^{\text{eq,w/o}} = \frac{\Gamma_s}{C_1 \Gamma_\phi}$ is the expression for N_γ^{eq} calculated without accounting for the Schwinger effect. This equation does not have a solution for all regions of parameter space; for some values of m_ϕ and α , it is simply impossible for the system to reach equilibrium. This represents the case where the suppression of axion decay is so great that the photons will never build up to the point where they come into equilibrium with the axions. While the number of photons will reach or approach some peak value (which may be found by solving $\frac{\Gamma_{\text{Schw}}}{\Gamma_{e^\pm}} = N_{e^+e^-}^{\text{shutoff}}$ for N_γ), the number of axions will continue growing unbounded. This is reflected mathematically by the fact that $C_1 \Gamma'_\phi N_\gamma$ has some maximum attainable value, and, if this maximum value is less than Γ_s , then N_ϕ will increase without bound. This will eventually result in the black hole spinning down to the point where superradiance ceases. These regions of parameter space where the system is unstable are shown on Fig. 2.

In regions of parameter space where the system is stable, the equilibrium photon number is enhanced by a factor of $\frac{\Gamma_\phi}{\Gamma'_\phi}$. This enhancement is plotted in Fig. 3. Interestingly, for the majority of parameter space (where equilibrium is possible), this enhancement is negligible. For these regions, the behavior of the BLAST may be modeled without considering the impact of the Schwinger effect. However, we can see that the enhancement to the photon number (and, consequently, the luminosity) increases somewhat as one approaches the region of parameter space where the system becomes unstable. Thus there is a small region of parameter space, located right next to the region where BLASTs become unstable, where the BLASTs are stable but enhanced. It is in this region where we would expect to find the strongest stable BLASTs.

V. CONCLUSION

When an axion laser, such as a BLAST, becomes sufficiently strong, it can produce an electric field close to the critical Schwinger limit, resulting in the creation of electron-positron pairs. This has three effects on the dynamics

Stable and Unstable Regions of Parameter Space

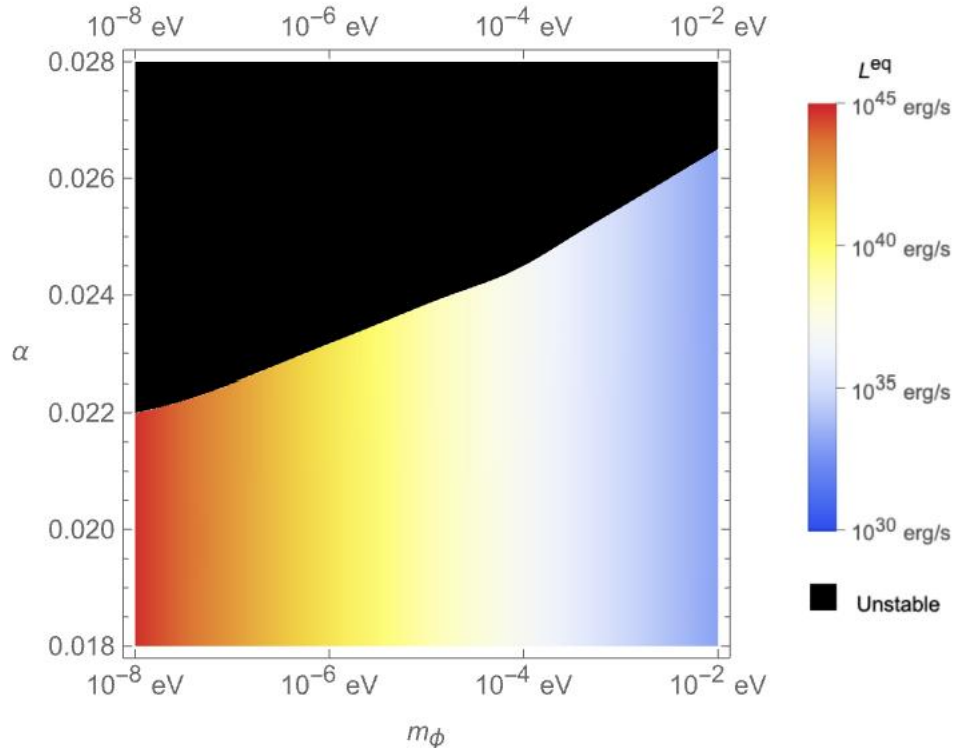


FIG. 2. Plot of the αm_ϕ plane of parameter space. The other parameters were taken to be $\tilde{a} = .7$ and $K = 1$. For larger values of α and smaller values of m_ϕ , the system is unstable, represented by the black-colored region of parameter space. In this region, the electron-positron plasma suppresses the axion decay so much that the photon number never becomes large enough to halt the growth of the axion number. The axion number therefore continues to grow superradiantly, causing the black hole to spin down until it is no longer superradiant. In the colored regions of parameter space, it is possible for the system to reach equilibrium, and the equilibrium luminosity is plotted. Especially for light axions, these luminosities are extremely high, making BLASTs potentially significant for future experiments. In the shaded region of parameter space, L^{eq} depends on both α and m_ϕ , but the dependence on α is too small to see on this plot.

of the photon and axion number: photons are lost as their energy is converted into electrons and positrons; electrons and positrons annihilate into photons, but with a higher energy than the photons produced by axion decay; and the buildup of an electron-positron plasma imparts an effective mass on the photon, slowing the rate of axion decay. We found that the third is the dominant phenomenon. How this alters the behavior of a BLAST depends on its parameters, specifically its values of α and m_ϕ .

To summarize, the parameter space of a BLAST may be divided into three regions:

- **Unenhanced:** In this region, the electron-positron plasma produced by the Schwinger effect has a negligible impact on the dynamics of the BLAST, and the analysis from [18] applies.
- **Unstable:** In this region, the system never reaches equilibrium. While the photon number N_γ will increase after the onset of lasing, the buildup of an electron-positron plasma suppresses the axion decay rate, so that the axion number N_ϕ continues to rise. This unbounded growth continues until the black hole spins down, at which point the axion no longer experiences superradiant growth.
- **Enhanced:** In between the previous two regions, the BLAST has an equilibrium state, but its equilibrium luminosity is enhanced compared to what is predicted in [18].

It is important to note that, in the first and third cases, the system will eventually reach its equilibrium state (likely undergoing damped oscillations about said equilibrium state). This is in contrast to what was predicted in [18], which speculated that the Schwinger effect would “restart” the system periodically. We therefore should only

Schwinger Enhancement to the Equilibrium Luminosity

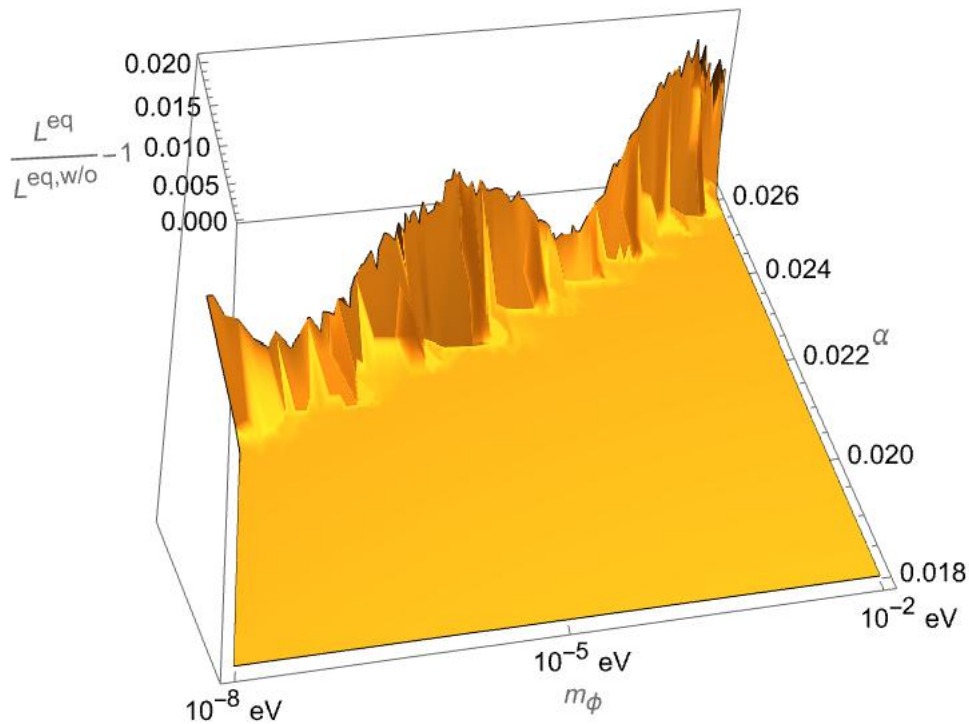


FIG. 3. Plot of the enhancement of the equilibrium luminosity against α and m_ϕ . L^{eq} is the equilibrium luminosity, while $L^{\text{eq,w/o}}$ is the equilibrium luminosity found in [18], i.e. ignoring the effects of Schwinger pairs. The same unstable region shown in Fig. 2 is also visible here. In the part of parameter space where an equilibrium state exists, we can see that the equilibrium luminosity is hardly enhanced at all, which means that the role of Schwinger production is negligible to the final state of the BLAST. However, close to the unstable region, there is a region where the enhancement becomes more significant. Note that computational constraints limit the resolution of the section of the plot with the greatest enhancement. This means that, even though the largest enhancement displayed on this plot is .02, it is likely that even greater enhancements can be achieved.

expect a BLAST to exhibit periodic behavior if we happen to observe it in its initial stages, before it has reached its equilibrium state.

It is worth noting that the equilibrium luminosities we have calculated are quite large in comparison to the mass of a primordial black hole. For example, if $m_\phi = 10^{-5}$ eV, then the largest a black hole can be while remaining in the stable region of parameter space is 6.5×10^{28} kg, and, if such a black hole were to remain in that equilibrium state continuously, it would evaporate after 7×10^5 years. In practice, such a black hole would undergo spin-down before this happened. Since the $2p$ -state has magnetic quantum number $m = 1$, each axion produced by superradiance carries with it angular momentum \hbar , and therefore the black hole's spin changes at a rate of $\frac{d\tilde{a}}{dt} = -\frac{\Gamma_s m_\phi}{\alpha M_{\text{BH}}} N_\phi$. As the black hole spins down, the superradiant growth of axions slows and eventually stops. Thus, BLASTs represent an important aspect of the behavior of rotating black holes. It has been shown that the emission of Hawking radiation will cause primordial black holes to randomly spin up [31]; once a primordial black hole's spin is high enough to initiate a BLAST, it will rapidly lose both mass and angular momentum. Understanding the dynamics of BLASTs is therefore essential to understanding the evolution of primordial black holes.

This paper has focused on the role of the Schwinger effect in one type of axion lasing system, namely, BLASTs. However, there are many other axion lasers that are of research interest (see [32] for a recent review). It is conceivable that the Schwinger effect may play a significant role in these axion lasers as well. Axion lasers are a promising method by which we might probe the existence of scalar dark matter. Understanding the role of the Schwinger effect in these processes may be necessary in order to develop accurate models of axion lasers.

An important caveat to these results is that our calculation of the rate of pair production involved two significant approximations: we ignored the role of both the magnetic field and the axion field. Therefore, all numerical results herein must be viewed as approximations, accurate to within a few orders of magnitude. A more careful analysis

would require the inclusion of both the magnetic field and the axion's enhancement to the Schwinger effect, as described in [27].

ACKNOWLEDGEMENTS

The author thanks Devin Walker and João Rosa for their helpful feedback. This work was supported by the National Science Foundation under grant OIA-2033382.

-
- [1] R. D. Peccei and H. R. Quinn, *Phys. Rev. Lett.* **38**, 1440 (1977).
- [2] S. Weinberg, *Phys. Rev. Lett.* **40**, 223 (1978).
- [3] F. Wilczek, *Phys. Rev. Lett.* **40**, 279 (1978).
- [4] C. B. Adams, N. Aggarwal, A. Agrawal, R. Balafendiev, C. Bartram, M. Baryakhtar, H. Bekker, P. Belov, K. K. Berggren, A. Berlin, C. Boutan, D. Bowring, D. Budker, A. Caldwell, P. Carena, G. Carosi, R. Cervantes, S. S. Chakrabarty, S. Chaudhuri, T. Y. Chen, S. Cheong, A. Chou, R. T. Co, J. Conrad, D. Croon, R. T. D'Agnolo, M. Demarteau, N. DePorzio, M. Descalle, K. Desch, L. D. Luzio, A. Diaz-Morcillo, K. Dona, I. S. Drachnev, A. Droster, N. Du, K. Dunne, B. Döbrich, S. A. R. Ellis, R. Essig, J. Fan, J. W. Foster, J. T. Fry, A. G. Rosso, J. M. G. Barceló, I. G. Irastorza, S. Gardner, A. A. Geraci, S. Ghosh, B. Giaccone, M. Giannotti, B. Gimeno, D. Grin, H. Grote, M. Guzzetti, M. H. Awida, R. Henning, S. Hoof, G. Hoshino, V. Irsic, K. D. Irwin, H. Jackson, D. F. J. Kimball, J. Jaeckel, K. Jakovcic, M. J. Jewell, M. Kagan, Y. Kahn, R. Khatiwada, S. Knirck, T. Kovachy, P. Krueger, S. E. Kuenstner, N. A. Kurinsky, R. K. Leane, A. F. Leder, C. Lee, K. W. Lehnert, E. W. Lentz, S. M. Lewis, J. Liu, M. Lynn, B. Majorovits, D. J. E. Marsh, R. H. Maruyama, B. T. McAllister, A. J. Millar, D. W. Miller, J. Mitchell, S. Morampudi, G. Mueller, S. Nagaitsev, E. Nardi, O. Noroozian, C. A. J. O'Hare, N. S. Oblath, J. L. Ouellet, K. M. W. Pappas, H. V. Peiris, K. Perez, A. Phipps, M. J. Pivovarov, P. Quilez, N. M. Rapidis, V. H. Robles, K. K. Rogers, J. Rudolph, J. Ruz, G. Rybka, M. Safdari, B. R. Safdi, M. S. Safronova, C. P. Salemi, P. Schuster, A. Schwartzman, J. Shu, M. Simanovskaia, J. Singh, S. Singh, K. Sinha, J. T. Sillis, M. Siodlaczek, M. S. Smith, W. M. Snow, A. V. Sokolov, A. Sonnenschein, D. H. Speller, Y. V. Stadnik, C. Sun, A. O. Sushkov, T. M. P. Tait, V. Takhistov, D. B. Tanner, F. Tavecchio, D. J. Temples, J. H. Thomas, M. E. Tobar, N. Toro, Y. D. Tsai, E. C. van Assendelft, K. van Bibber, M. Vandegar, L. Visinelli, E. Vitagliano, J. K. Vogel, Z. Wang, A. Wickenbrock, L. Winslow, S. Withington, M. Wooten, J. Yang, B. A. Young, F. Yu, K. Zhou, and T. Zhou, "Axion dark matter," (2023), arXiv:2203.14923 [hep-ex].
- [5] A. Arvanitaki, S. Dimopoulos, S. Dubovsky, N. Kaloper, and J. March-Russell, *Physical Review D* **81** (2010), 10.1103/physrevd.81.123530.
- [6] A. Arvanitaki and S. Dubovsky, *Physical Review D* **83** (2011), 10.1103/physrevd.83.044026.
- [7] R. Brito, V. Cardoso, and P. Pani, *Classical and Quantum Gravity* **32**, 134001 (2015).
- [8] A. Arvanitaki, M. Baryakhtar, S. Dimopoulos, S. Dubovsky, and R. Lasenby, *Physical Review D* **95** (2017), 10.1103/physrevd.95.043001.
- [9] H. Davoudiasl and P. B. Denton, *Physical Review Letters* **123** (2019), 10.1103/physrevlett.123.021102.
- [10] S. L. Detweiler, *Phys. Rev. D* **22**, 2323 (1980).
- [11] S. R. Dolan, *Physical Review D* **76** (2007), 10.1103/physrevd.76.084001.
- [12] R. Brito, V. Cardoso, and P. Pani, *Superradiance: New Frontiers in Black Hole Physics* (Springer International Publishing, 2020).
- [13] A. Arvanitaki, M. Baryakhtar, and X. Huang, *Physical Review D* **91** (2015), 10.1103/physrevd.91.084011.
- [14] D. Baumann, H. S. Chia, J. Stout, and L. t. Haar, *Journal of Cosmology and Astroparticle Physics* **2019**, 006–006 (2019).
- [15] J. D. Bekenstein and M. Schiffer, *Physical Review D* **58** (1998), 10.1103/physrevd.58.064014.
- [16] R. Alicki and A. Jenkins, *Annals of Physics* **395**, 69–83 (2018).
- [17] V. Balakumar, E. Winstanley, R. P. Bernar, and L. C. Crispino, *Physics Letters B* **811**, 135904 (2020).
- [18] J. G. Rosa and T. W. Kephart, *Physical Review Letters* **120** (2018), 10.1103/physrevlett.120.231102.
- [19] J. Schwinger, *Phys. Rev.* **82**, 664 (1951).
- [20] F. Gelis and N. Tanji, *Progress in Particle and Nuclear Physics* **87**, 1–49 (2016).
- [21] A. Ringwald, *Physics Letters B* **510**, 107–116 (2001).
- [22] R. Alkofer, M. B. Hecht, C. D. Roberts, S. M. Schmidt, and D. V. Vinnik, *Physical Review Letters* **87** (2001), 10.1103/physrevlett.87.193902.
- [23] B. S. Xie, Z. L. Li, and S. Tang, *Matter and Radiation at Extremes* **2**, 225 (2017), https://pubs.aip.org/aip/mre/article-pdf/2/5/225/13684815/225_1_online.pdf.
- [24] F. Hebenstreit, R. Alkofer, G. V. Dunne, and H. Gies, *Physical Review Letters* **102** (2009), 10.1103/physrevlett.102.150404.
- [25] A. D. Panferov, S. A. Smolyansky, A. Otto, B. Kampfer, D. B. Blaschke, and L. Juchnowski, *The European Physical Journal D* **70** (2016), 10.1140/epjd/e2016-60517-y.
- [26] M. Ruf, G. R. Mocken, C. Müller, K. Z. Hatsagortsyan, and C. H. Keitel, *Physical Review Letters* **102** (2009), 10.1103/physrevlett.102.080402.
- [27] V. Domcke, Y. Ema, and K. Mukaida, *Journal of High Energy Physics* **2021** (2021), 10.1007/jhep05(2021)001.

- [28] F. Hebenstreit, “Schwinger effect in inhomogeneous electric fields,” (2011), arXiv:1106.5965 [hep-ph].
 [29] R. Svensson, *Astrophys. J.* **258**, 321 (1982).
 [30] P. S. Coppi and R. D. Blandford, *Monthly Notices of the Royal Astronomical Society* **245**, 453 (1990).
 [31] Q. Taylor, G. D. Starkman, M. Hinczewski, D. P. Mihaylov, J. Silk, and J. de Freitas Pacheco, (2024), arXiv:2403.04054 [gr-qc].
 [32] L. Chen and T. W. Kephart, *Universe* **10**, 24 (2024), arXiv:2311.16453 [hep-ph].

Appendix: Behavior of functions of χ

The dimensionless parameter χ represents the rate at which electrons and positrons are accelerated to relativistic velocities by radiation pressure. A number of quantities may be expressed solely as a function of χ , and in this appendix we establish the mathematical tools to analyze these functions.

It is helpful to rescale quantities of length by a factor of $\frac{\chi}{\Delta r}$; we label quantities that have been rescaled in this way with a hat, e.g. $\hat{\rho}_0 = \chi \frac{\rho_0}{\Delta r}$. With this notation, the relation between the location of an electron or positron’s creation and the time it takes for that electron or positron to exit the $2p$ -cloud may be written as

$$\chi - \hat{\rho}_0 = \sqrt{\hat{T}_{e^\pm}^2 - 1} - \tan^{-1} \sqrt{\hat{T}_{e^\pm}^2 - 1}, \quad (\text{A.1})$$

and the escape rate is

$$\Gamma_{e^\pm} = \frac{\chi^3}{6 \int_0^\chi \hat{T}_{e^\pm} \hat{\rho}_0 d\hat{\rho}_0} \Gamma_\gamma. \quad (\text{A.2})$$

This makes it clear that $\frac{\Gamma_{e^\pm}}{\Gamma_\gamma}$ is a function only of χ . Its asymptotic behavior may be derived by noting that, in the limit $\chi \rightarrow \infty$, the arctangent term in eq. (A.1) becomes insignificant, and so

$$\Gamma_{e^\pm} \xrightarrow{\chi \rightarrow \infty} \frac{\chi^3}{6 \int_0^\chi \sqrt{(\chi - \hat{\rho}_0)^2 + 1} d\hat{\rho}_0} \Gamma_\gamma, \quad (\text{A.3})$$

which may be evaluated to find that $\Gamma_{e^\pm} \rightarrow \Gamma_\gamma$, which is also what one would expect physically.

An integral which appears in pair annihilation, when written using hat notation, is

$$\Gamma_{\text{ann}} V = \frac{8}{\chi^2} \int_0^\chi d\hat{\rho} \int_0^{\hat{\rho}} d\hat{\rho}_{0e^+} \int_0^{\hat{\rho}} d\hat{\rho}_{0e^-} \frac{\hat{\rho}_{0e^+} \hat{\rho}_{0e^-}}{\hat{\rho}^3} |v_{e^+} - v_{e^-}| \sigma(v_{\text{com}}), \quad (\text{A.4})$$

where

$$\hat{\rho} - \hat{\rho}_{0e^\pm} = \frac{v_{e^\pm}}{\sqrt{1 - v_{e^\pm}^2}} - \tan^{-1} \frac{v_{e^\pm}}{\sqrt{1 - v_{e^\pm}^2}}. \quad (\text{A.5})$$

The asymptotic behavior of $\Gamma_{\text{ann}} V$ may be examined in a similar manner to Γ_{e^\pm} , although in this case it is convenient to examine $\frac{d(\chi^2 \Gamma_{\text{ann}} V)}{d\chi}$:

$$\frac{d(\chi^2 \Gamma_{\text{ann}} V)}{d\chi} \xrightarrow{\chi \rightarrow \infty} \frac{8}{\chi^3} \int_0^{\frac{\chi}{\sqrt{\chi^2+1}}} d v_{e^+} \int_0^{\frac{\chi}{\sqrt{\chi^2+1}}} d v_{e^-} \gamma_{e^+}^3 \gamma_{e^-}^3 \left(\chi - \frac{v_{e^+}}{\sqrt{1 - v_{e^+}^2}} \right) \left(\chi - \frac{v_{e^-}}{\sqrt{1 - v_{e^-}^2}} \right) |v_{e^+} - v_{e^-}| \sigma(v_{\text{com}}). \quad (\text{A.6})$$

We may convert the double integral into a single integral by differentiating three times:

$$\frac{d^3}{d\chi^3} \chi^3 \frac{d(\chi^2 \Gamma_{\text{ann}} V)}{d\chi} \xrightarrow{\chi \rightarrow \infty} 16 \int_0^{\frac{\chi}{\sqrt{\chi^2+1}}} d v_{e^-} \gamma_{e^-}^3 \left(3 + \left(\chi - \frac{v_{e^-}}{\sqrt{1 - v_{e^-}^2}} \right) \frac{d}{d\chi} \right) \left(|v_{e^+} - v_{e^-}| \sigma(v_{\text{com}}) \Big|_{v_{e^+} = \frac{\chi}{\sqrt{\chi^2+1}}} \right) \quad (\text{A.7})$$

In the limit $\chi \rightarrow \infty$, the integrand becomes

$$\gamma_{e^-}^3 \left(3 + \left(\chi - \frac{v_{e^-}}{\sqrt{1 - v_{e^-}^2}} \right) \frac{d}{d\chi} \right) \left(|v_{e^+} - v_{e^-}| \sigma(v_{\text{com}}) \Big|_{v_{e^+} = \frac{\chi}{\sqrt{\chi^2+1}}} \right) \xrightarrow{\chi \rightarrow \infty} \frac{3(1 + v_{e^-}) \ln \left(2\chi \sqrt{\frac{1 - v_{e^-}}{1 + v_{e^-}}} \right)}{8\chi^2 (1 - v_{e^-}^2)^{\frac{3}{2}}} \sigma_T. \quad (\text{A.8})$$

When this is integrated, we arrive at our asymptotic form for $\Gamma_{\text{ann}}V$:

$$\Gamma_{\text{ann}}V \xrightarrow{\chi \rightarrow \infty} \frac{3(\ln \chi)^2}{2\chi^2} \sigma_T. \quad (\text{A.9})$$

Eq. (49) follows straightforwardly.